**Cell Reports, Volume *34***

## Supplemental information

# Blockade of 6-phosphogluconate dehydrogenase generates $CD8^+$ effector T cells with enhanced anti-tumor function

**Saeed Daneshmandi, Teresa Cassel, Penghui Lin, Richard M. Higashi, Gerburg M. Wulf, Vassiliki A. Boussiotis, Teresa W.-M. Fan, and Pankaj Seth**

## Supplemental Information:

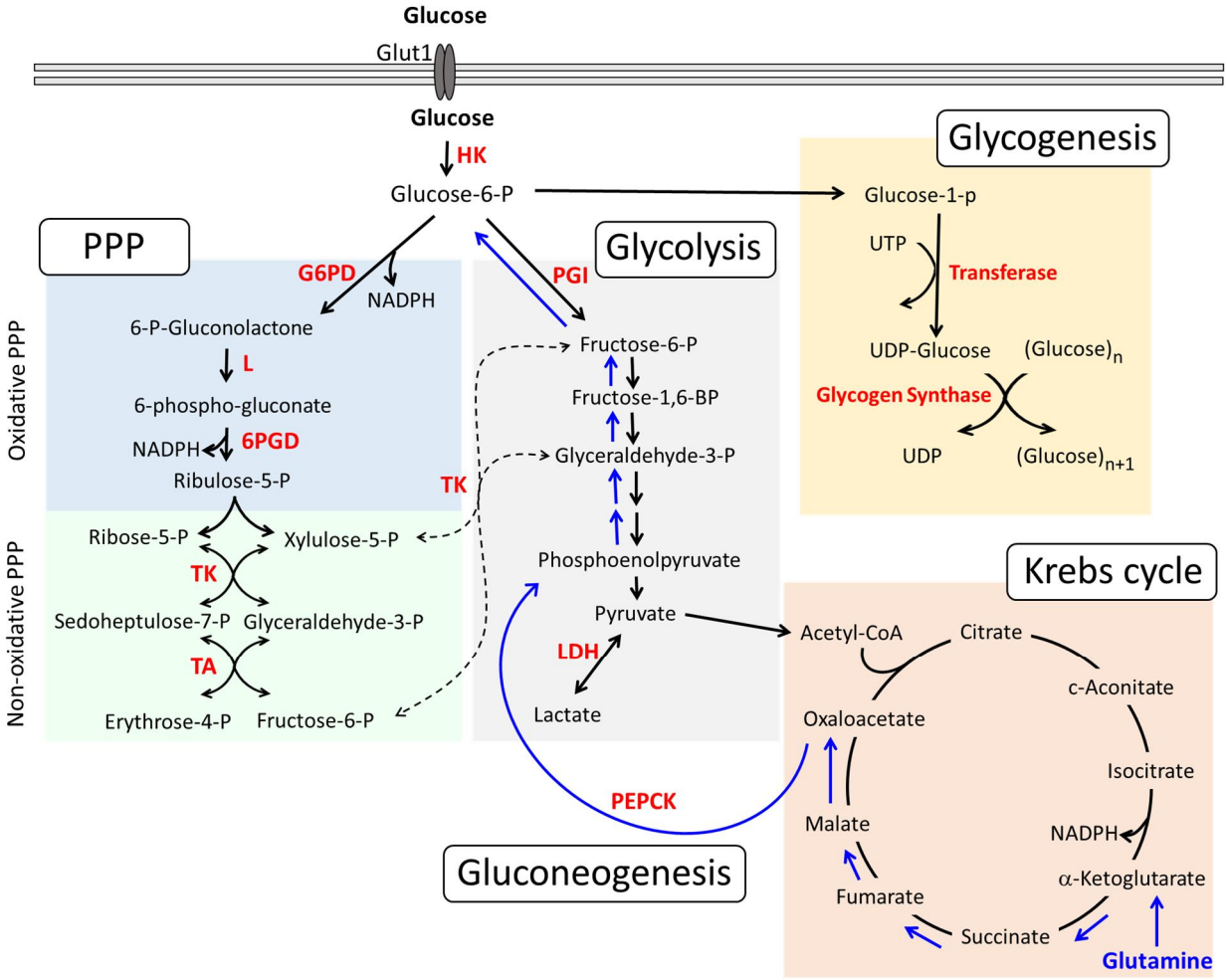


**Figure S1: Schematic diagram interconnecting PPP, glycolysis, gluconeogenesis, glycogenesis, and the Krebs cycle. Related to Figure 1 and 5.** After transported into the cell, glucose is converted to glucose-6-phosphate (glucose-6-P) by the enzyme hexokinase (HK). Subsequently, glucose-6-P can be catabolized in glycolysis, directed to PPP to generate ribose-5-phosphate (ribose-5-P) and NADPH for anabolic and anti-oxidation metabolism, and converted to glucose-1-phosphate (glucose-1-P) to fuel glycogen synthesis. The product of glycolysis, pyruvate, is fed into the Krebs cycle for further oxidation. Glutamine is fed into the Krebs cycle via α-ketoglutarate, which can fuel gluconeogenesis as shown by the blue arrows. HK: Hexokinase; G6PD: Glucose-6-phosphate Dehydrogenase; L: Lactonase; 6PGD: 6-phosphogluconate Dehydrogenase; TK: Transketolase; TA: Transaldolase; PGI: Phosphoglucose Isomerase; LDH: Lactate Dehydrogenase; PEPCK: Phosphoenolpyruvate carboxykinase.

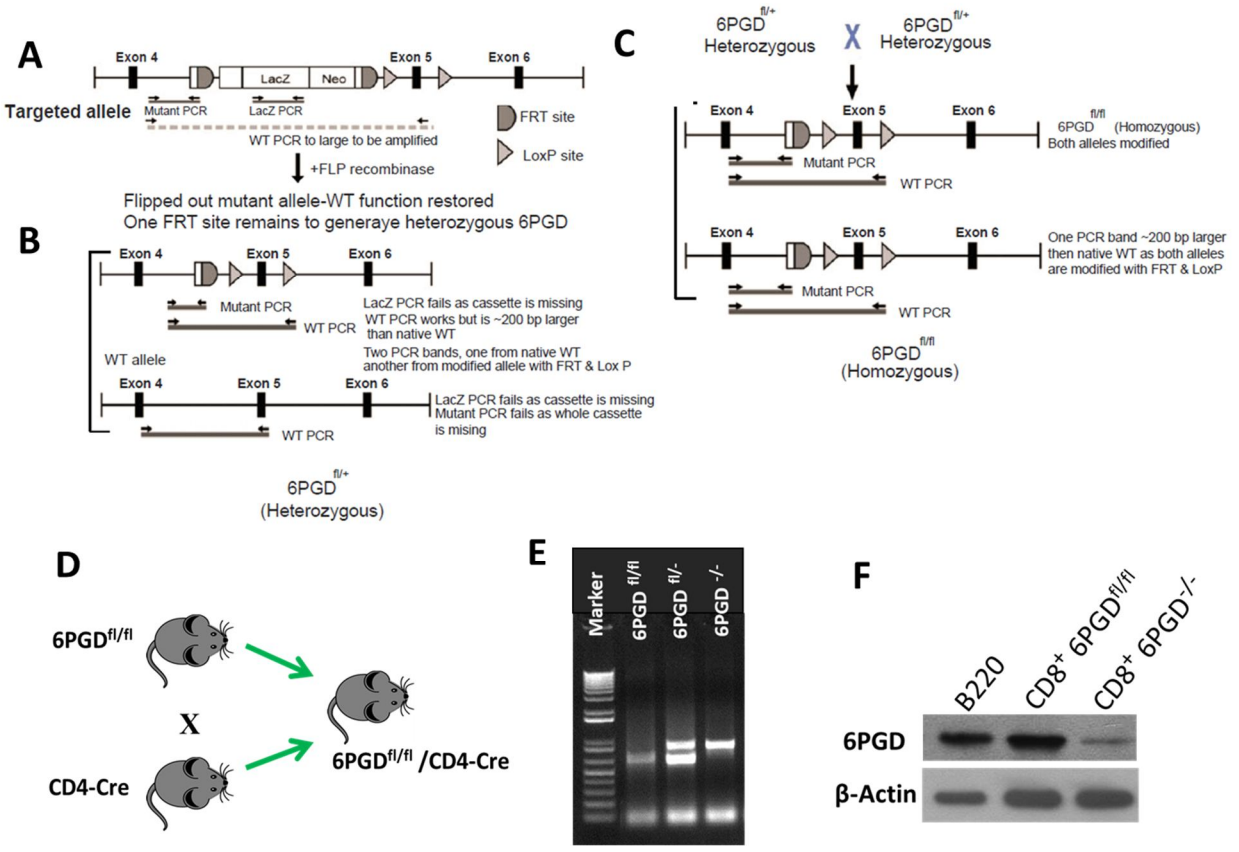


**Figure S2: Generation of 6PGD$^{fl/fl}$CD4$^{cre}$ (6PGD$^{-/-}$) mice. Related to Figure 1. (A)** Schematic representation of a targeted allele: The targeting strategy leads to the insertion of the SA–ßgeo–pA cassette into the intron between exons 4 and 5 of 6PGD, which disrupts gene function, and reports the expression of the targeted gene. The targeted 6PGD exon 5 is flanked by loxP sites. (Key: FRT, target site for FLP recombinase; loxP, target site for Cre-recombinase; SA, splice acceptor; ßgeo, ß-galactosidase/neomycin phosphotransferase fusion gene; pA, polyadenylation sequence). **(B)** Conditional allele after excision of the SA–ßgeo–pA cassette by FLP recombinase deleted mouse strain referred to as 6PGD$^{fl/+}$ since it represents heterozygous status of modified 6PGD allele. **(C)** Heterozygous mice were crossed to generate homozygous 6PGD$^{fl/fl}$. **(D)** 6PGD$^{fl/fl}$ mice were crossed with mice carrying Cre recombinase under the control of the CD4 promoter (CD4-Cre) to generate 6PGD$^{fl/fl}$/CD4-Cre. **(E)** PCR validation of the 6PGD$^{fl/+}$/CD4-Cre and 6PGD$^{fl/fl}$/CD4-Cre mice. **(F)** Western blot analysis CD8$^{+}$ T cells from 6PGD$^{fl/fl}$/CD4-Cre (6PGD$^{-/-}$) and 6PGD$^{fl/fl}$ mice.

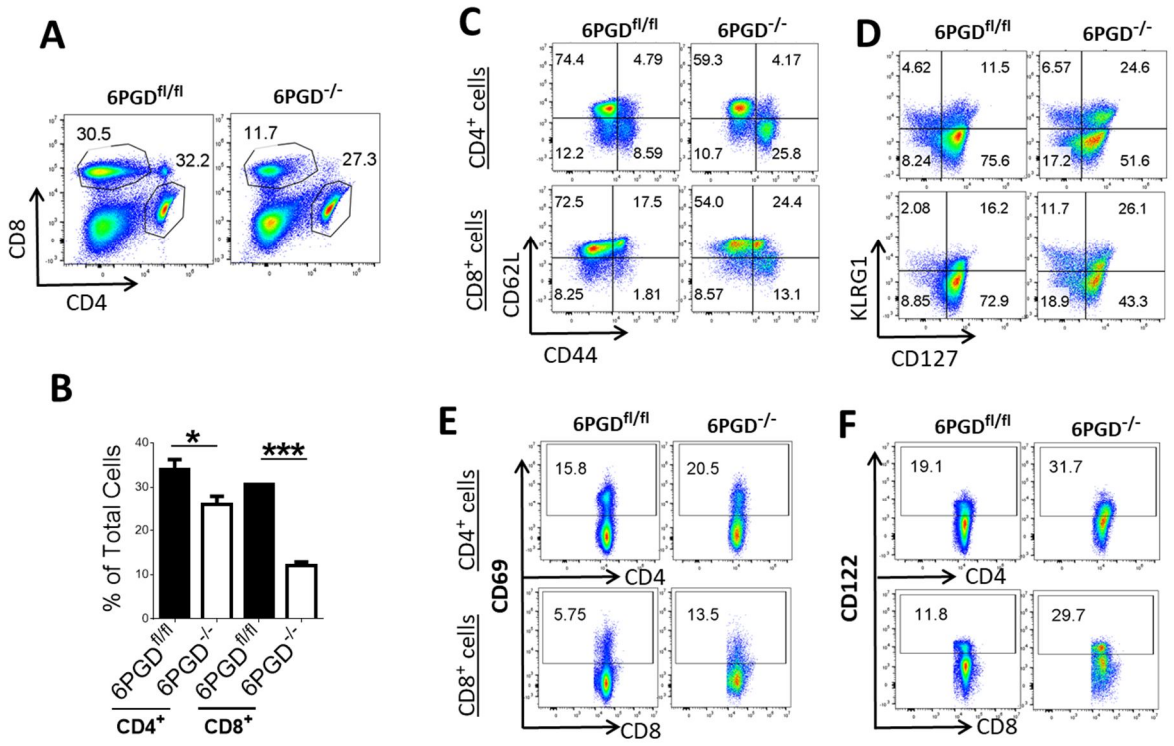


**Figure S3: CD4$^+$ and CD8$^+$ T cells in the lymph nodes of 6PGD$^{-/-}$ mice display an activated phenotype. Related to Figure 1. (A-B)** Lymph node cells were collected from 6PGD$^{-/-}$ and 6PGD$^{fl/fl}$ mice and CD4$^+$ and CD8$^+$ T cells were assessed by flow cytometry **(A)**. Representative dot plots **(A)** and average values of three independent experiments **(B)** are shown. **(C-D)** Lymph node cells were collected from 6PGD$^{fl/fl}$ and 6PGD$^{-/-}$ mice and expression of the indicated combination of markers (CD44/CD62L and KLRG1/CD127) was assessed by flow cytometry to identify naïve (CD62L$^{high}$ CD44$^{low}$), effector (CD62L$^{low}$ CD44$^{high}$) and memory (CD62L$^{high}$ CD44$^{high}$) cells on gated CD4$^+$ and CD8$^+$ populations. Representative dot plots are shown. Results are representative of two independent experiments. **(E-F)** Lymph nodes were collected from 6PGD$^{-/-}$ and 6PGD$^{fl/fl}$ mice and expression of CD69 and CD122 on gated CD4$^+$ and CD8$^+$ T cells was assessed by flow cytometry. Representative dot plots are shown. Results are representative of two independent experiments. Error bars represent ± SEM.*: p <0.05; ***: p <0.001.

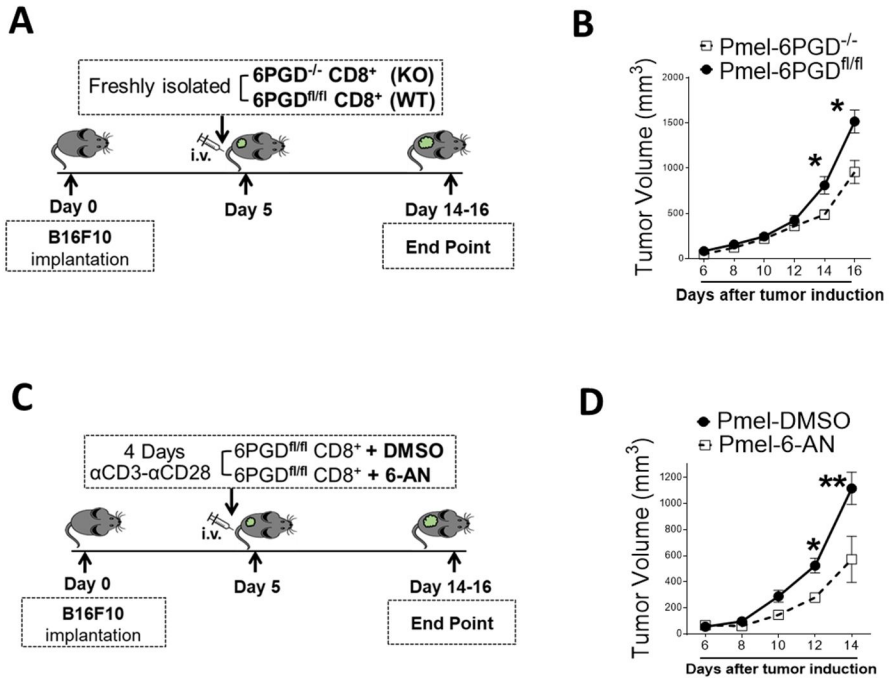


**Figure S4: Genetic ablation or pharmacologic inhibition of 6PGD induces CD8$^+$ T cells with enhanced effector function against pmel B16-F10 tumor in vivo. Related to Figure 3. (A-B)** CD8$^+$ T cells from pmel/6PGD$^{-/-}$ and pmel/6PGD$^{fl/fl}$ mice were cultured with αCD3+αCD28 mAbs-plus-IL-2 (20 IU/ml) for 4 days and were subsequently adoptively transferred to congenic mice (CD45.1$^+$) bearing B16F10 melanoma tumors **(A)**. Tumor size was measured every 48 hours and tumor volume was calculated **(B)**. Results are representative of two independent experiments with n=9 mice per group. (**C-D**) CD8$^+$ T cells were isolated from pmel/6PGD$^{fl/fl}$ mice and were stimulated in vitro with αCD3+αCD28 mAbs-plus-IL-2 (20 IU/ml) for 4 days in the presence of 6-AN or vehicle control (DMSO). Cells were subsequently adoptively transferred to congenic mice (CD45.1$^+$) bearing B16F10 melanoma tumors. (**C**) Tumor growth was evaluated by measuring size every 2 days and tumor volume was calculated. Results are representative of two independent experiments with n=10 mice per group. Error bars represent ± SEM. *: p <0.05; **: p <0.01.

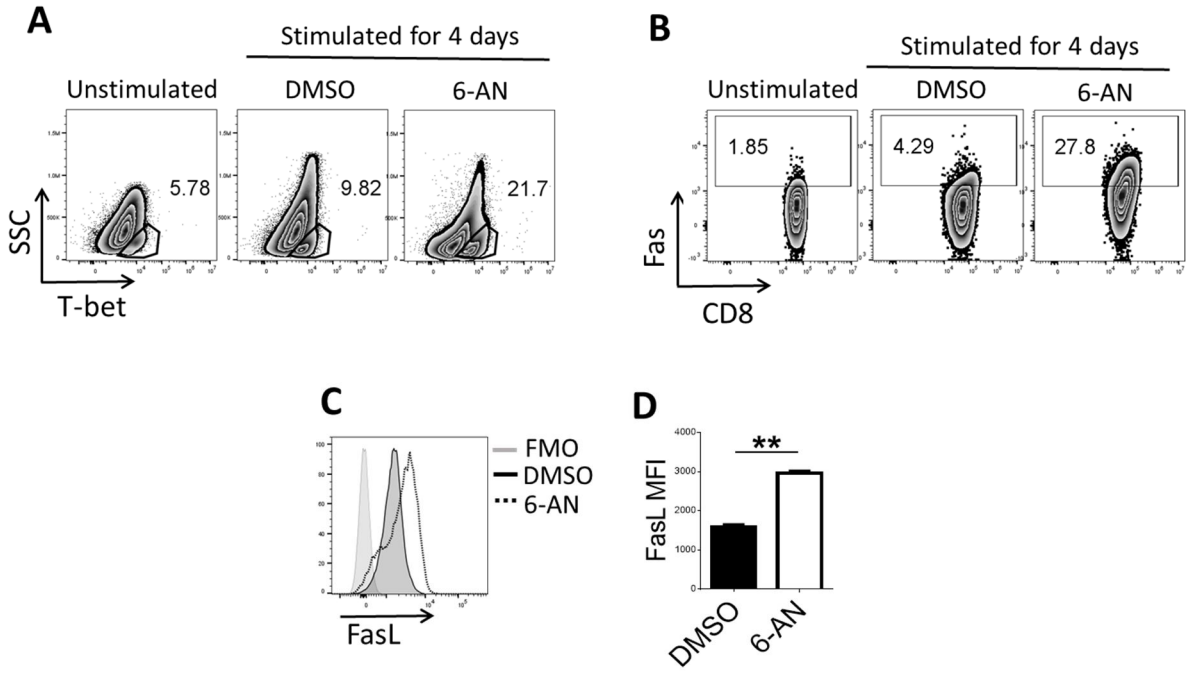


**Figure S5: Effect of 6-AN on naïve CD8$^+$ T cells stimulated in vitro. Related to Figure 4. (A-D)** Naïve CD8$^+$ T cells were isolated from C57BL/6 WT mice and were cultured in vitro in the presence of αCD3+αCD28 mAbs and IL-2 for 4 days in the presence of 6-AN (10 μM) or vehicle control (DMSO). Expression of T-bet **(A)**, Fas **(B)** and FasL **(C, D)** was determined by flow cytometry. Results are representative of three independent experiments with n=4 per experiment. Error bars represent ± SEM. **: $p < 0.01$.

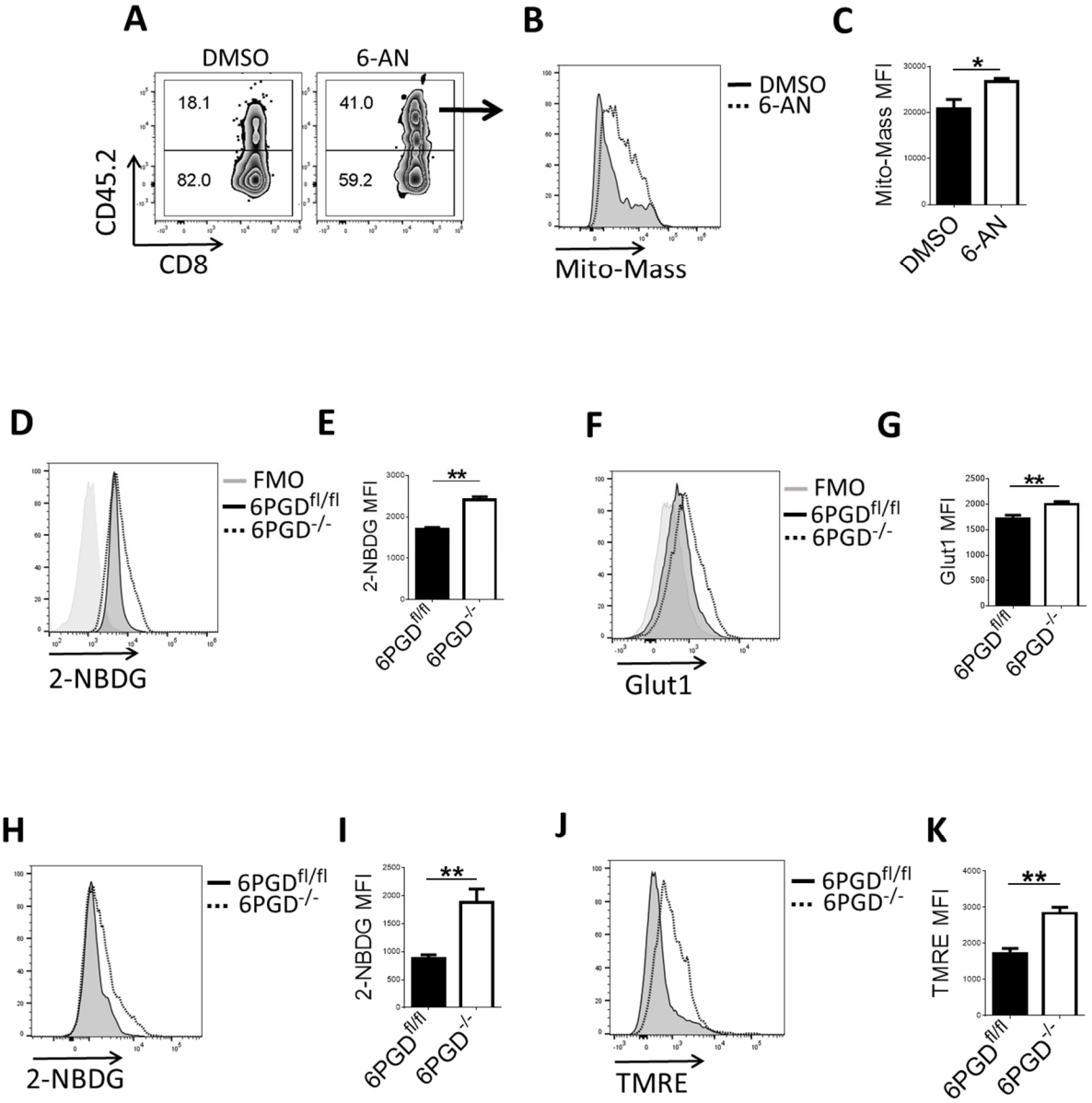


**Figure S6: CD8$^+$ T cells metabolic characteristics. Related to Figure 3 and 5. (A-C)** Infiltration and mitochondrial status of adoptively transferred naïve CD8$^+$ 6PGD$^{fl/fl}$ pmel$^+$ cells treated with 6-AN. **(A)** Fractions of adoptively transferred T cells (CD45.2$^+$) in TILs 10 days after adoptively transfer of 6PGD$^{fl/fl}$ pmel$^+$ CD8$^+$ cells were cultured with αCD3+αCD28 mAbs plus-IL-2 for 4 days in the presence of 6-AN or vehicle control (DMSO) and were subsequently transferred to (CD45.1$^+$) congenic mice. Fractions of in vitro-treated CD45.2$^+$ T cells in TILs was assessed 10 days after adoptive transfer. **(B-C)** Histoplots and bar graph representative of mitochondrial mass (MFI) for CD45.2$^+$ infiltrated TILs on day 10 post adoptive transfer of 6-AN or DMSO pre-treated CD8$^+$ T cells. Results are representative of two independent experiments with n=6 mice per group. **(D-G)** Glucose uptake by CD8$^+$ T cells from 6PGD$^{-/-}$ and 6PGD$^{fl/fl}$ mice. **(D-F)** Splenic CD8$^+$ T cells

from 6PGD$^{-/-}$ and 6PGD$^{fl/fl}$ mice were isolated and expression of Glut1 on their surface is shown as histogram and MFI bar graph. **(F-G)** Glucose uptake capacity was examined by uptake of 2-NBDG on CD8$^{+}$ T cells from 6PGD$^{-/-}$ and 6PGD$^{fl/fl}$ mice. Results are representative of two independent experiments with n=3 per experiment. **(H-K)** Glucose uptake and mitochondrial membrane potential of pmel/6PGD$^{fl/fl}$ and 6PGD$^{-/-}$ CD8$^{+}$ T cells as co-culture with B16 melanoma tumor cells in vitro. **(H-I)** pmel/6PGD$^{fl/fl}$ and pmel/6PGD$^{-/-}$ CD8$^{+}$ T cells were co-cultured for 20 hr with B16-F10 melanoma cells, media was washed away, and the co-culture was exposed to low concentration of 2-NBDG. The results are shown as histogram and calculated MFI for CD8$^{+}$ T cells. **(J-K)** Similarly, mitochondrial membrane potential was assessed by TMRE fluorescence and results are shown as histoplot and MFI bar graph. Results are representative of two independent experiments with n=4 per experiment. Glut1: Glucose transporter 1; 2-NBDG: 2-deoxy-2-[(7-nitro-2,1,3-benzoxadiazol-4-yl)amino]-D-glucose. Error bars represent ± SEM. *: $p < 0.05$; **: $p < 0.01$.

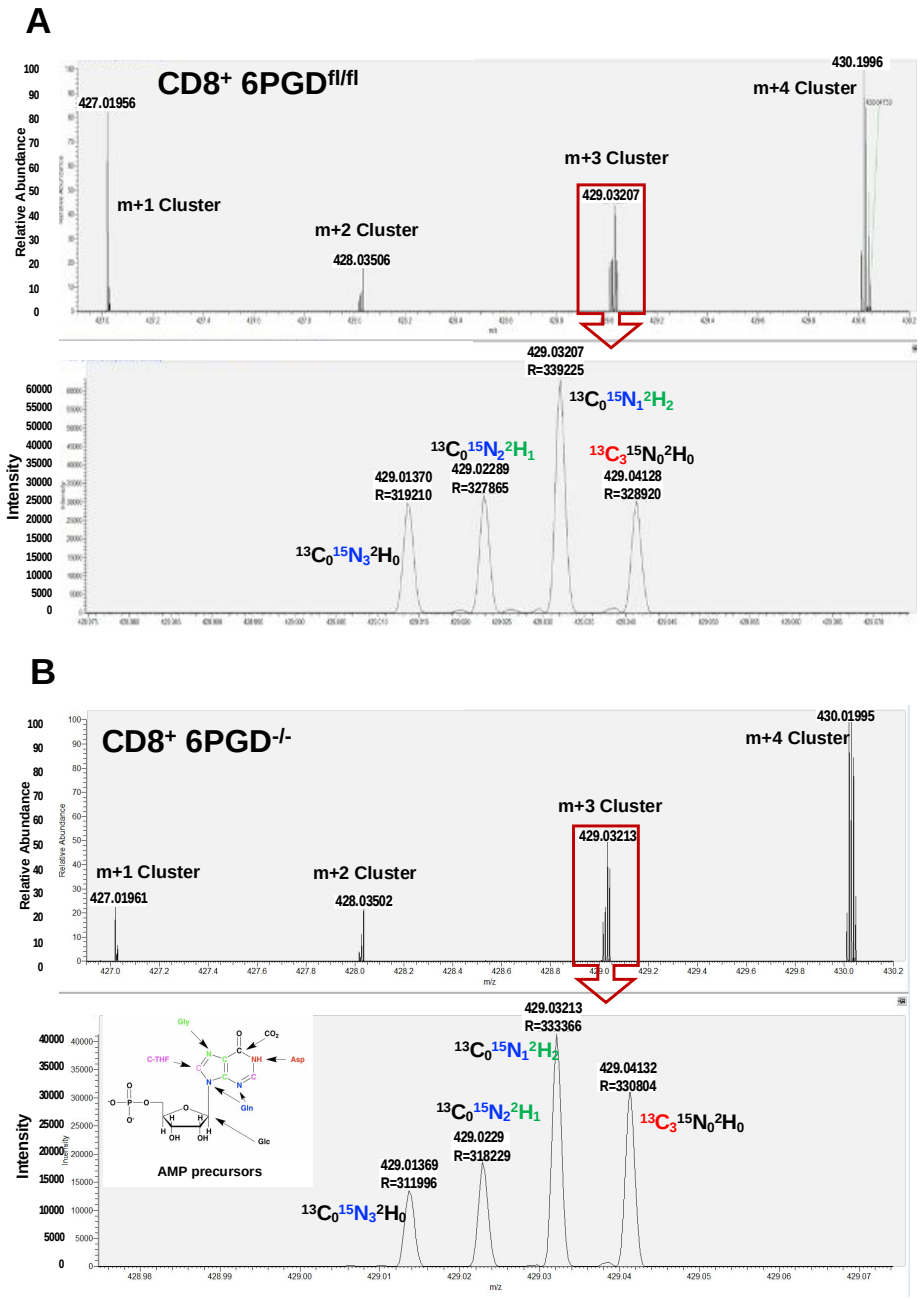


**Figure S7: UHRMS[1] resolution of simultaneous $^{13}C$, $^{15}N$, and $^{2}H$ in isotopologues of ATP with the same nominal m/z of 429.0x. Related to Figure 5.** Top panels show the first four isotopic enrichment clusters of UHRMS[1] spectra of ATP from IC-UHRMS[1] runs of one each CD8$^+$ T cells with wildtype (6PGD$^{fl/fl}$, **A**) and 6PGD knockout (6PGD$^{-/-}$, **B**), both in $D_7$-Glc + $^{13}C_5$,$^{15}N_2$-Gln dual tracer, triple-isotopic label experiments. The bottom panels show the expanded spectra of 4 ATP isotopologues with the same nominal m/z of 429.0x, which is ~3 m/z higher (m+3 cluster) than that the $^{12}C$,$^{14}N$,$^{1}H$-isotopologue (monoisotopic cluster). They were fully baseline resolved and assigned to $^{13}C_0{}^{15}N_3{}^{2}H_0$, $^{13}C_0{}^{15}N_2{}^{2}H_1$, $^{13}C_0{}^{15}N_1{}^{2}H_2$, and $^{13}C_3{}^{15}N_0{}^{2}H_0$, based on the IC retention time and the exact mass of ATP with a loss of phosphate, which were confirmed by a parallel ATP standard run. **R** refers to the mass resolution achieved with each isotopologue; the exact m/z's

shown are raw values prior to post-run m/z correction. Also shown in **B** is a diagram illustrating carbon and nitrogen origin of AMP (same origins as for ATP), i.e. the ribosyl unit from glucose (Glc), three carbons of adenine ring from Gly and formyl-tetrahydrofolate (C-THF), two nitrogens from Gln, and one nitrogen from Asp. The abundance of $^{13}C_3$-ATP indicates its synthesis from $^{13}C_5$,$^{15}N_2$-Gln via Gly, C-THF, and/or ribose, all of which are produced via gluconeogenesis (GNG). The relatively higher enrichment of $^{13}C_3$-ATP in 6PGD$^{-/-}$ versus WT cells is consistent with enhanced fueling of ATP synthesis via GNG in 6PGD$^{-/-}$ cells.

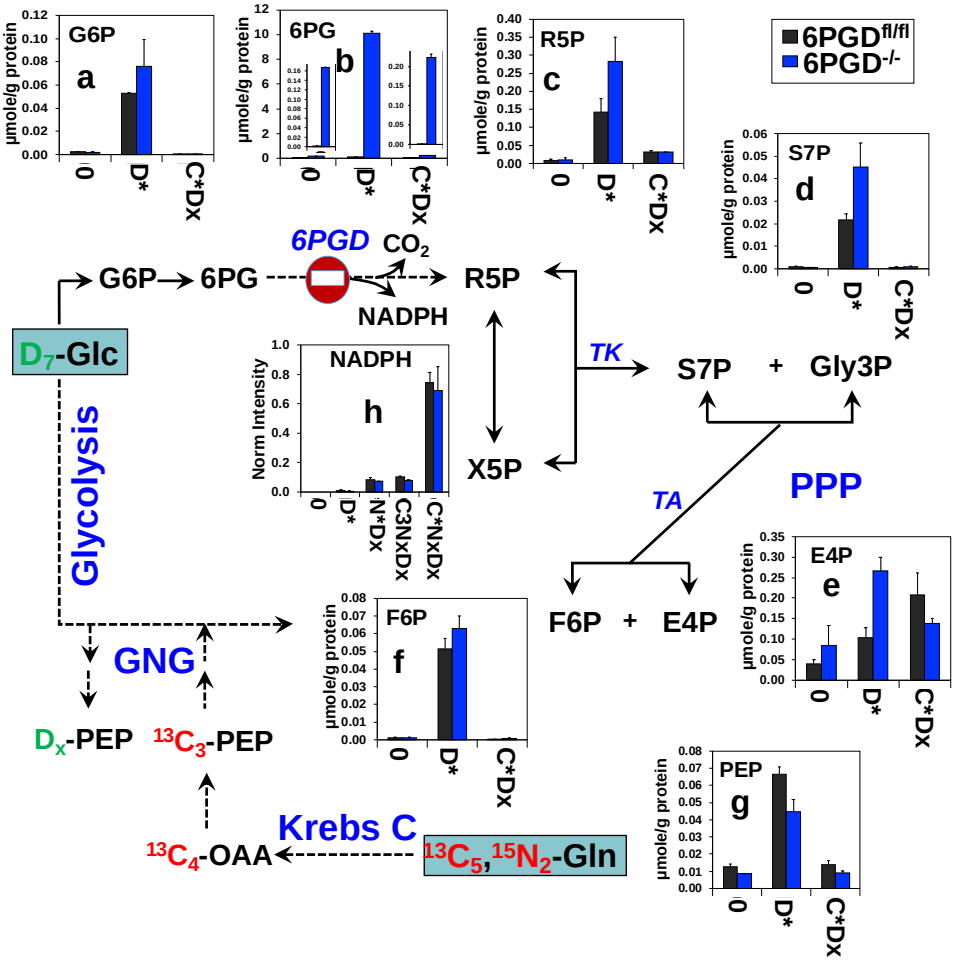


**Figure S8: 6PGD$^{-/-}$ ablation results in enhanced non-oxidative PPP and diversion of gluconeogenic carbons to PPP. Related to Figure 5.** The cell extracts (n=2) in Figure 5 were analyzed by IC-UHRMS as µmole/g protein. Legend in X-axis: 0 = unlabeled; Dx = sum of $D_1$ to $D_x$ or Glc-derived species; C*Dx = sum of $^{13}C$ labeled species with 0-x number of D; N*Dx = sum of $^{15}N$ labeled species with 0-x number of D; C3NxDx = sum of $^{13}C_3$ with 0-x number of D and $^{15}N$, which could reflect incorporation of GNG product into the ribose unit of NADPH; C*NxDx = sum of $^{13}C$ labeled species with 0-x number of $^{15}N$ and D. G6P, glucose-6-phosphate; 6-PG, 6-phosphogluconate; R5P, ribose-5-phosphate; S7P, sedoheptulose-7-phosphate; Gly3P, glyceraldehyde-3-phosphate; X5P, xylulose-5-phosphate; E4P, erythrose-4-phosphate; F6P, fructose-6-phosphate. Error bars represent ± SEM.

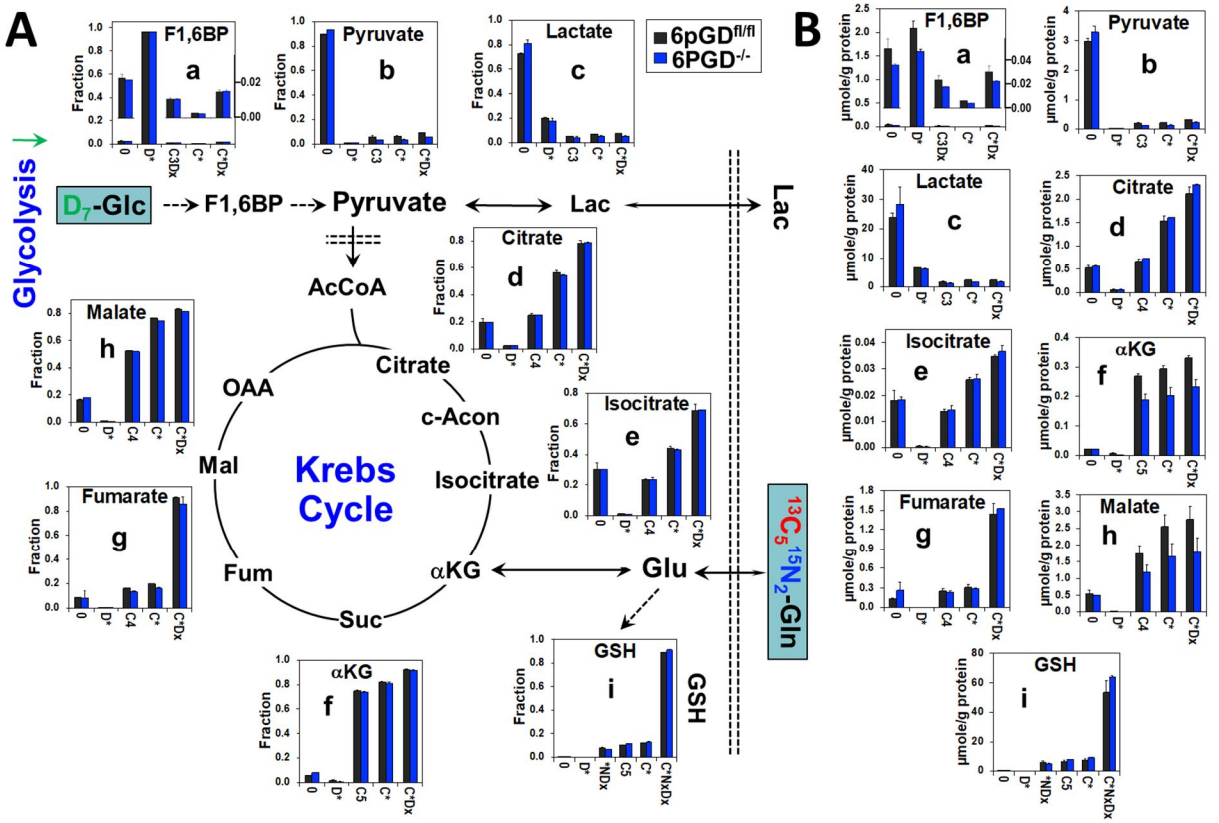


**Figure S9: 6PGD$^{-/-}$ ablation has negligible effect on glycolysis, the Krebs cycle, and glutathione synthesis. Related to Figure 5.** The cell extracts in Figure 5 were analyzed by IC-UHRMS for glycolytic and Krebs cycle metabolites as well as glutathione (GSH). Fractional enrichment and μmole/g protein data are shown in **A** and **B**, respectively. Results were generated from two independent experiments. Legend in X-axis: 0 = unlabeled; Dx = sum of $D_1$ to $D_x$ or Glc-derived species; C3Dx = sum of $^{13}C_3$ with 0-x number of D, which could indicate incorporation of gluconeogenesis (GNG) product into sugar phosphates; C* = sum of $^{13}C$ labeled only or Gln-derived species; C*Dx = sum of $^{13}C$ labeled species with 0-x number of D; N*Dx = sum of $^{15}N$ labeled species with 0-x number of D; C*NxDx = sum of $^{13}C$ labeled species with 0-x number of $^{15}N$ and D. F1,6BP, fructose-1,6-bisphosphate; Lac, lactate; AcCoA, acetyl CoA; c-Acon, cis-aconitate; αKG, α-ketoglutarate; Suc, succinate; Fum, fumarate; Mal, malate; OAA, oxaloacetate; GSH, glutathione. Error bars represent ± SEM.

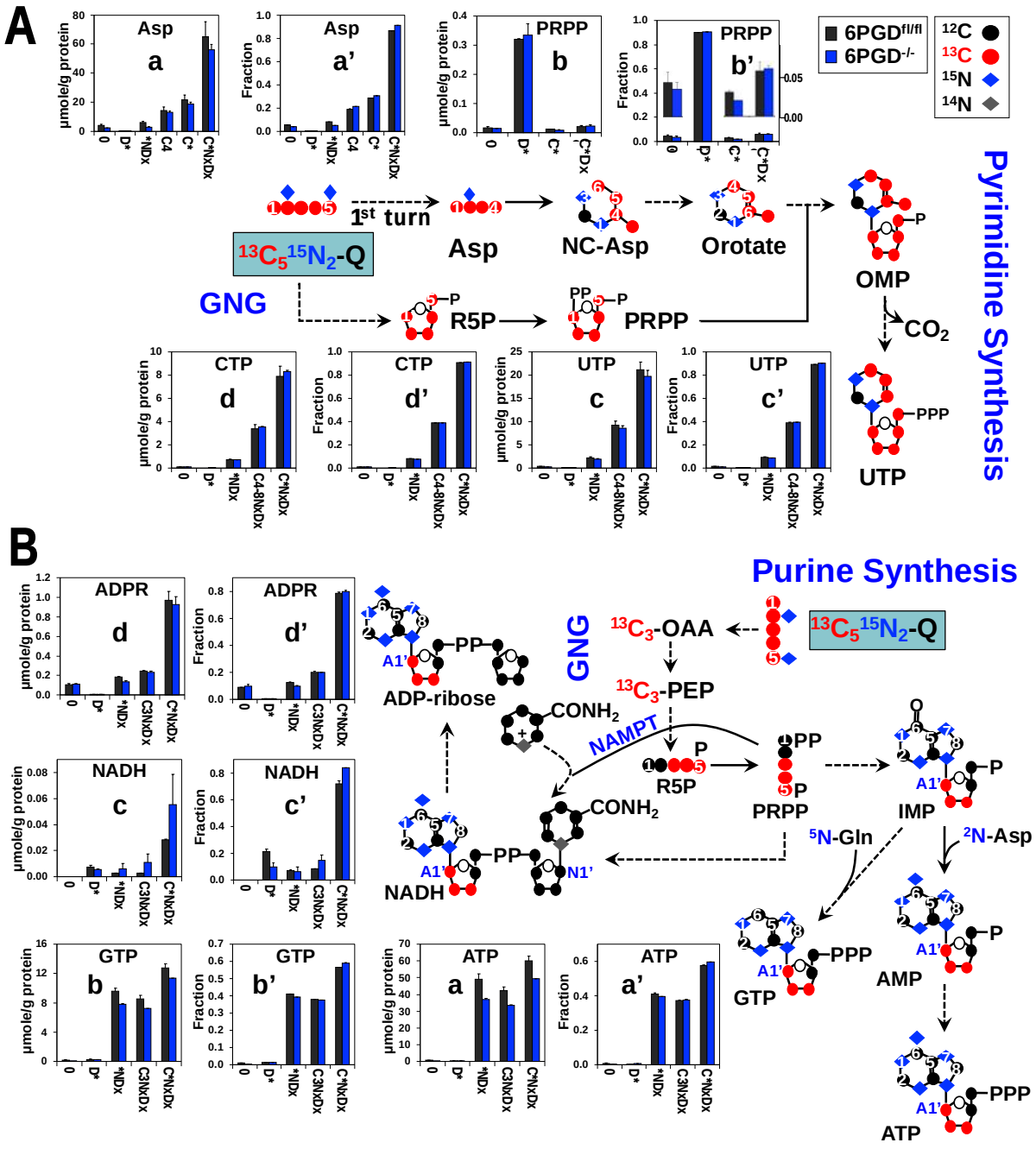


**Figure S10: Nucleotide biosynthesis is sustained in 6PGD deficient CD8$^+$ T cells. Related to Figure 5.** The same polar extracts from Figure 5 were analyzed for nucleotides and related metabolites by IC-UHRMS. Shown in **A** and **B** are changes in the levels (**a**-**d**) and fractional enrichment (**a'**-**d'**) of selected intermediates and products of the pyrimidine and purine nucleotide/dinucleotide synthesis pathways, respectively. Also shown is the $^{13}$C and $^{15}$N tracing from the Gln tracer to pyrimidine and purine nucleotides via GNG and the nucleotide synthesis pathways. Not all labeled species are shown. Comparing 6PGD$^{fl/fl}$ and 6PGD$^{-/-}$ CD8$^+$ T cells, there was no significant attenuation in the incorporation of D, $^{13}$C, and/or $^{15}$N into pyrimidine nucleotide metabolites (**A**). This was also the case for purine nucleotides and dinucleotides (**B**). Labels in

X-axis describe the same series of mass isotopologues as in **Figure 5**. In addition, C4-8NxDx (sum of $^{13}C_{4-8}$ species with 0-x number of $^{15}N$ and D) in **A** reflects $^{13}C$ incorporation into the ribose unit of UTP and CTP via GNG since the maximal number of $^{13}C$ in the pyrimidine ring is 3. Abbreviations used are: Asp, aspartate; PRPP, phosphoribosyl pyrophosphate; UTP: uridine triphosphate; CTP: cytidine triphosphate; IMP: inosine monophosphate; ADPR, ADP-ribose; NADH: nicotinamide adenine dinucleotide; GTP: quanosine triphosphate; ATP: adenosine triphosphate; GNG: gluconeogenesis. Error bars represent ± SEM.

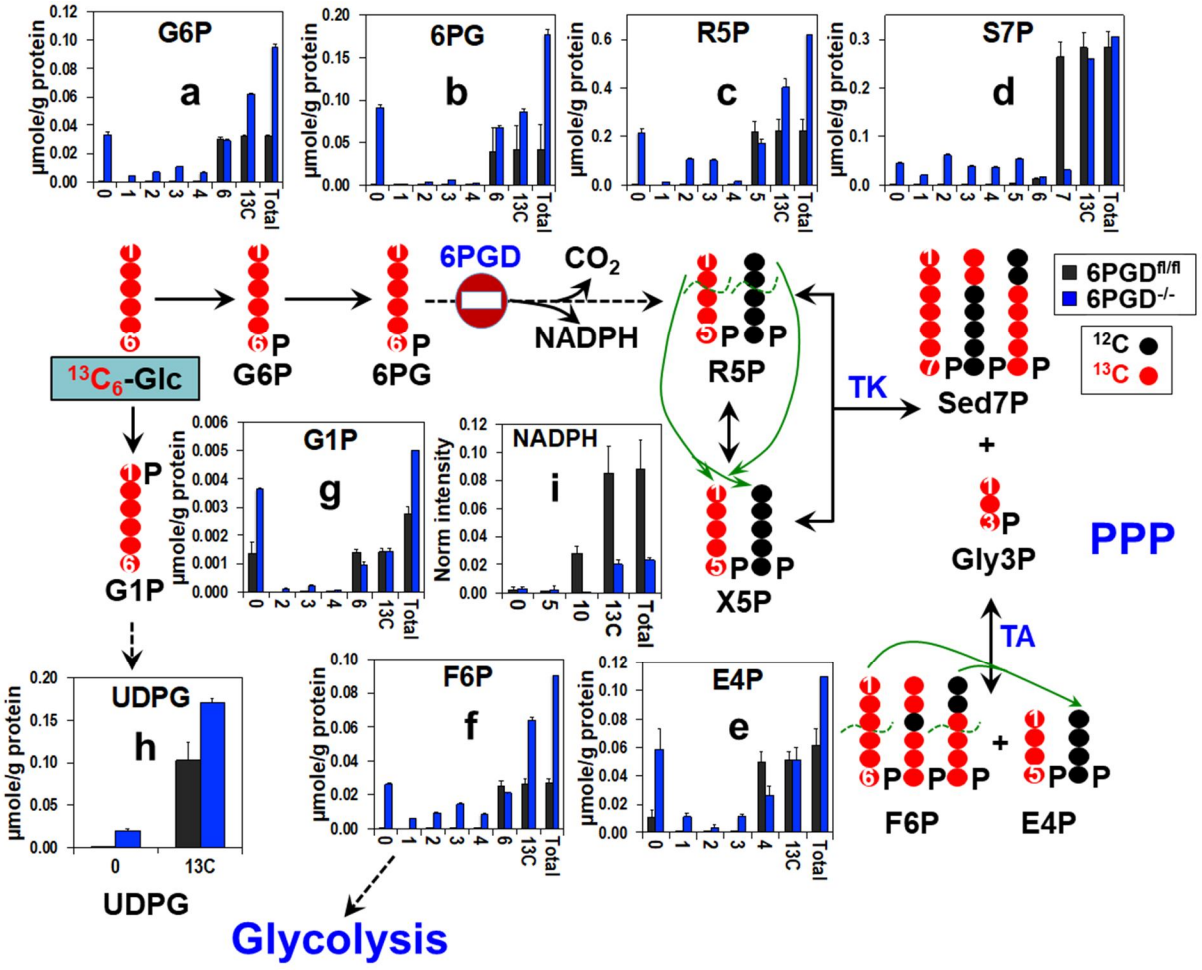


**Figure S11: $^{13}C_6$-glucose tracer study of unsorted 6PGD$^{-/-}$ CD8$^+$ T cells confirms the suppression of 6PGD and activation of the non-oxidative PPP. Related to Figure 5.** Total CD8$^+$ T cells were isolated from 6PGD$^{-/-}$ and 6PGD$^{fl/fl}$ mice and stimulated with αCD3+αCD28 in the presence of $^{13}C_6$-Glc for 48 hrs. Isotope labeling patterns of metabolites of cell extracts were analyzed by IC-UHRMS. Diagram demonstrate the conversion of $^{13}C_6$-Glc into the metabolites of PPP and glycogen synthesis intermediates. Results are representative of two independent experiments. G6P, glucose-6-phosphate; 6-PG, 6-phosphogluconate; R5P, ribose-5-phosphate; S7P, sedoheptulose-7-phosphate; Gly3P, glyceraldehyde-3-phosphate; X5P, xylulose-5-phosphate; E4P, erythrose-4-phosphate; F6P, fructose-6-phosphate; G1P, glucose-1-phosphate; UDPG, Uridine diphosphate glucose. Error bars represent ± SEM.

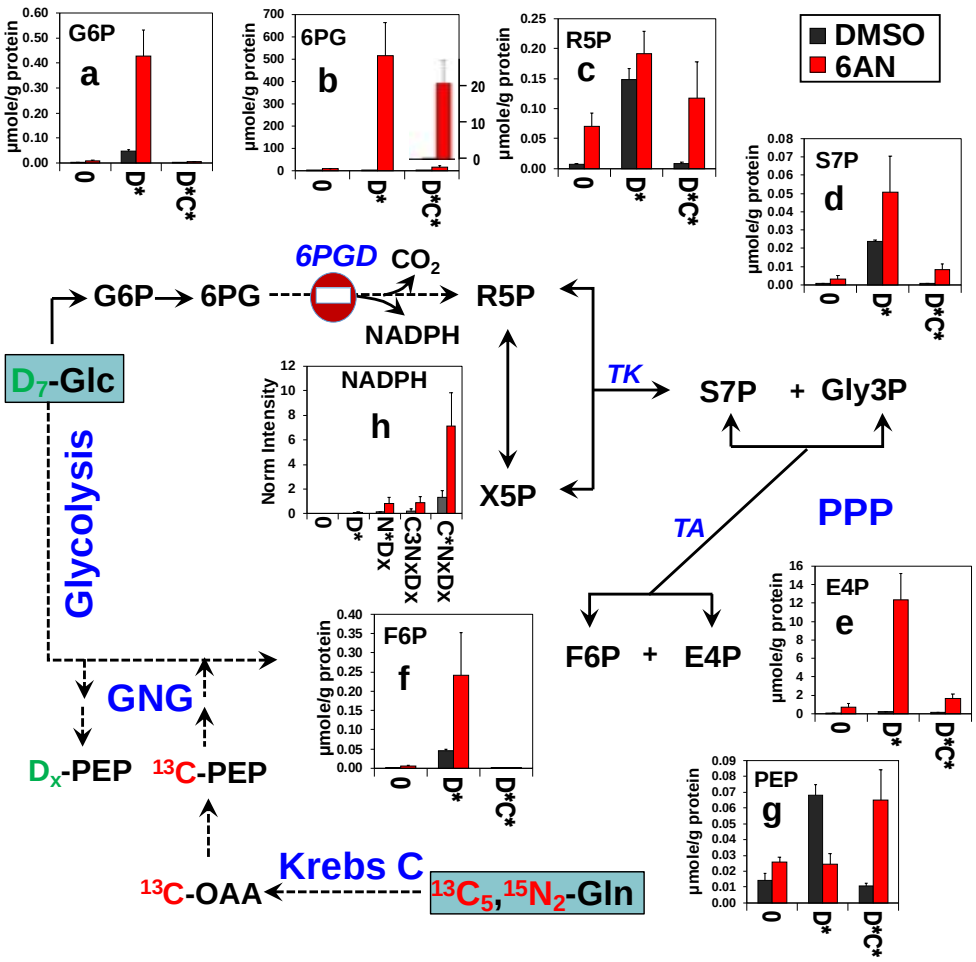


**Figure S12: 6PGD inhibition by 6-AN results in enhanced non-oxidative PPP and diversion of gluconeogenic carbons to PPP. Related to Figure 5.** The same batch of naïve CD8$^+$ T cells from Figure 5 were treated with 6-AN or the DMSO vehicle in the presence of dual $D_7$-Glc + $^{13}C_5$,$^{15}N_2$-Gln tracers for 4 days. The polar extracts were analyzed by IC-UHRFTMS. indicates inhibition of 6PGD and activation of the non-oxidative PPP by 6-AN. All abbreviations are the same as in Figure 5. Error bars represent ± SEM.

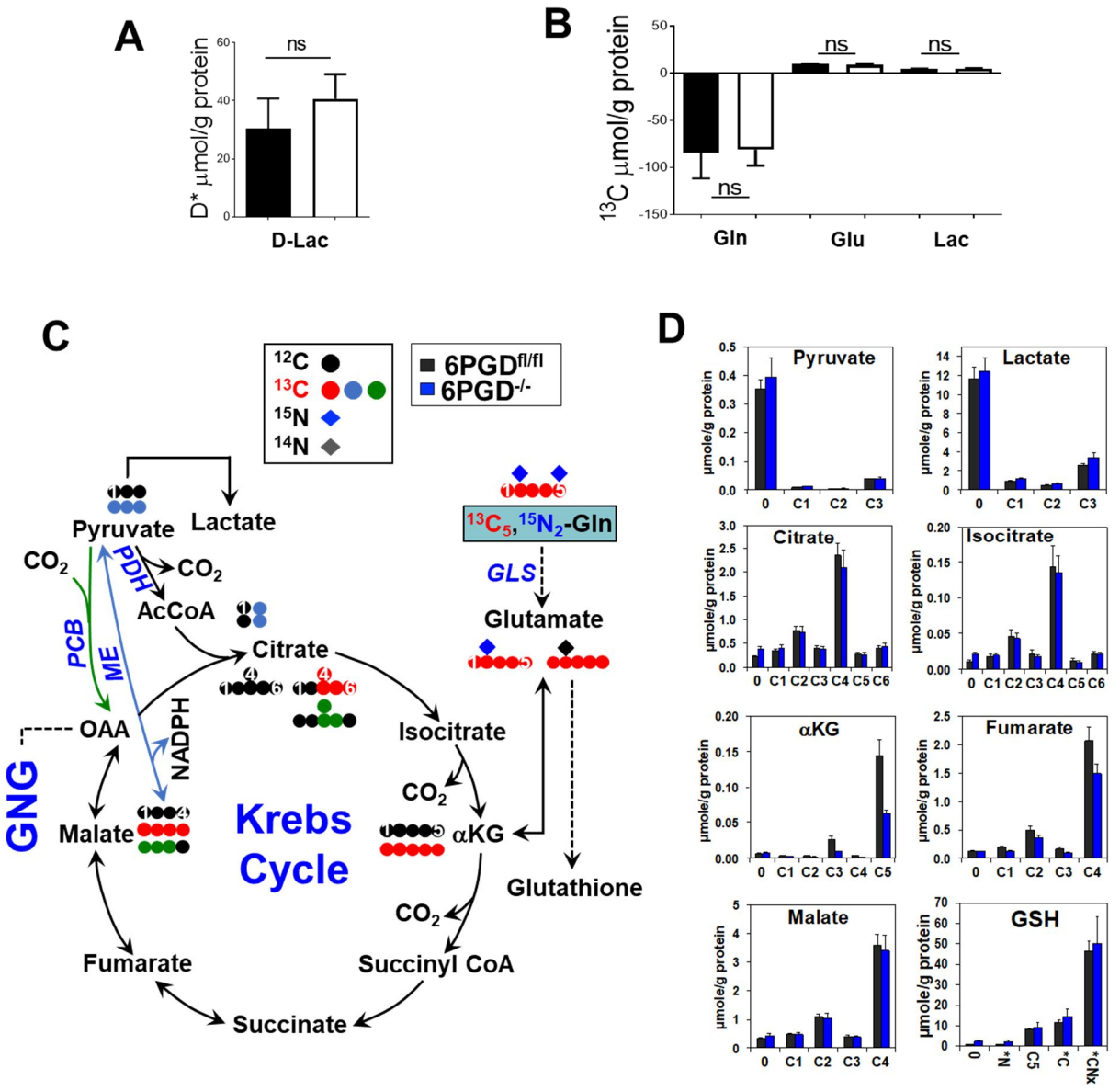


**Figure S13: $^{13}C_5$,$^{15}N_2$-Gln tracer study of 6PGD$^{-/-}$ ablation in unsorted CD8$^+$ T cells shows comparable effect on the labeling patterns of metabolites as those from the dual $D_7$-Glc+$^{13}C_5$,$^{15}N_2$-Gln tracer study. Related to Figure 5. (A-B)** Media culture from the same set of experiments in Figure 5 was analyzed by NMR. **(A)** Release of D labeled lactate showed a trend of increase in 6PGD$^{-/-}$ CD8$^+$ T cells but it was not statistically significant. **(B)** There was no significant changes in the consumption of the Gln tracer or the release of the $^{13}$C-Glu and -Lac products into the media. **(C-D)** Total CD8$^+$ T cells were isolated from 6PGD$^{-/-}$ and 6PGD$^{fl/fl}$ mice and stimulated with αCD3+αCD28 in the presence of $^{13}C_5$,$^{15}N_2$-Gln for 48 hrs. Panel **C** traces the fate of $^{13}$C and $^{15}$N via the glutaminase (GLS) and the first Krebs cycle activities. Metabolites were analyzed by IC-UHRMS and shown as µmole/g protein data in **D**. Results are representative of two independent experiments. Lac: Lactate; Gln: Glutamine; Glu: Glutamate. PDH: pyruvate dehydrogenase; ME: malic enzyme; PCB: pyruvate carboxylase; GNG: gluconeogenesis; AcCoA, acetyl CoA; αKG, α-ketoglutarate; OAA, oxaloacetate; GSH, glutathione. Error bars represent ± SEM.

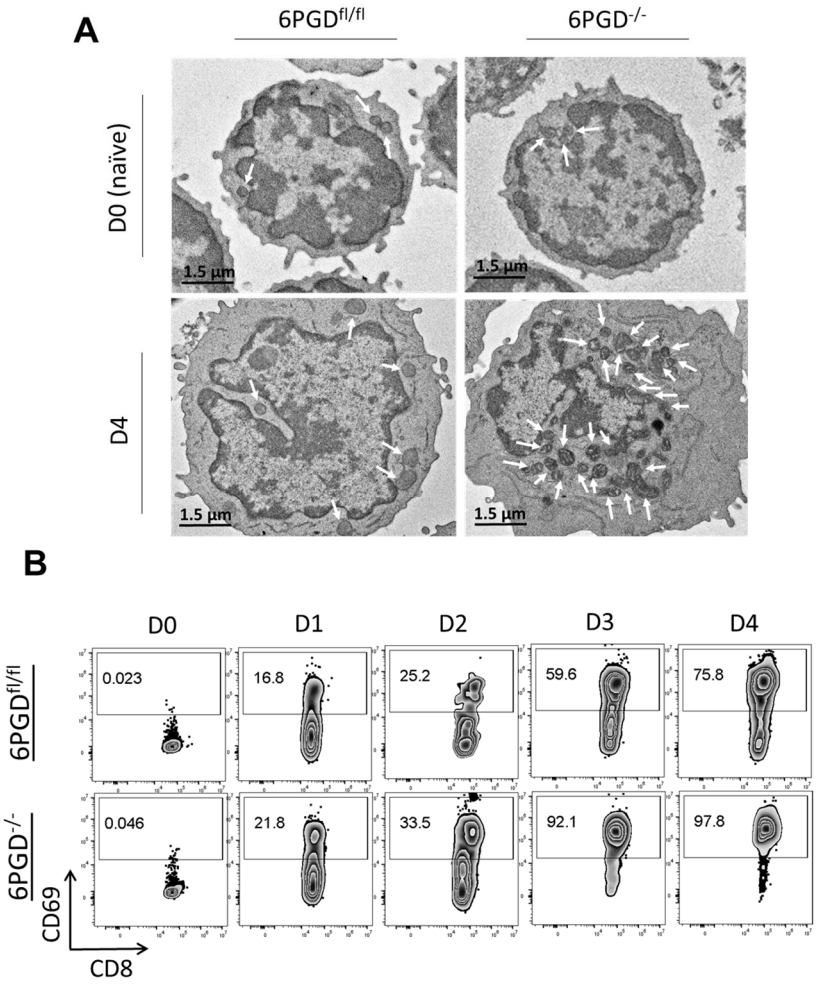


**Figure S14: 6PGD$^{-/-}$ CD8$^{+}$ T cells have higher mitochondria numbers and higher CD69 marker expression during activation**. **Related to Figure 6 and 7. (A)** Splenic naïve (CD62L$^{high}$ CD44$^{low}$) CD8$^{+}$ T cells from 6PGD$^{-/-}$ and 6PGD$^{fl/fl}$ mice were isolated, stimulated with αCD3+αCD28 mAbs-plus-IL-2 (20 IU/ml) for 4 days and analyzed by at day 0 (naïve) and 4 days post stimulation by electron microscopy (EM). Representative images of mitochondria number per cell are shown. Scale bars are mentioned in the figures. **(B)** Naïve CD8$^{+}$ T cells from 6PGD$^{-/-}$ and 6PGD$^{fl/fl}$ mice were stimulated for 4 days with αCD3+αCD28 mAbs-plus-IL-2 (20 IU/ml) and expression of CD69 was examined by flow cytometry. Results are representative of two independent experiments with n=3 per experiment.